

1 **Arctic Ozone Loss Climatology from Solar Occultation and Microwave Limb**
2 **Sounding Instruments**

3 C. S. Singleton^{1,2}, C. E. Randall^{1,3}, V.L. Harvey¹, M. P. Chipperfield⁴, W. Feng⁴, G.L.
4 Manney^{5,6}, C.T. McElroy^{7,8}

5

6 ¹ Laboratory for Atmospheric and Space Physics, UCB 392, University of Colorado,
7 Boulder, CO 80309-0392, USA

8 ² Now a AAAS Science and Technology Policy Fellow at the National Science
9 Foundation, 4201 Wilson Boulevard, Arlington, VA 22230, USA

10 ³ Also at the Department of Atmospheric and Oceanic Sciences, University of
11 Colorado.

12 ⁴ Institute for Atmospheric Science, School of Earth and Environment, University of
13 Leeds, Leeds LS2 9JT, UK

14 ⁵ Jet Propulsion Laboratory, California Institute of Technology, Pasadena CA 91109

15 ⁶ Department of Physics, New Mexico Institute of Mining and Technology, Las
16 Vegas, NM, 87701, USA

17 ⁷ Meteorological Service of Canada, Environment Canada, 4905 Dufferin St.,
18 Downsview, ON,
19 Canada, M3H 5T4

20 ⁸ Department of Physics, University of Toronto, 60 St. George St., Toronto, ON,
21 Canada, M5S1A7

22

23 Correspondence: C. S. Singleton (cynthia.singleton@lasp.colorado.edu)

- 1 Running Title: Arctic ozone loss climatology
- 2 Running Author: C. S. Singleton et al.
- 3

1 **Abstract:**

2 Interannual variability in lower stratospheric Arctic ozone loss is investigated
3 for the Arctic winters of 94/95 through 04/05. The chemical transport model Passive
4 Subtraction technique is used to infer chemical ozone loss from observations from the
5 Upper Atmosphere Research Satellite and Earth Observing System Microwave Limb
6 Sounders, Polar Ozone and Aerosol Measurement II/III, Stratospheric Aerosol and
7 Gas Experiment II/III, Improved Limb Atmospheric Spectrometer, Halogen
8 Occultation Experiment, Atmospheric Chemistry Experiment Fourier Transform
9 Spectrometer, and Measurement of Aerosol Extinction in the Stratosphere and
10 Troposphere Retrieved by Occultation instruments. These loss inferences indicate
11 that in most years the maximum loss occurred between 400 and 500K (~15-20 km),
12 except for warm winters where the maximum loss occurred between 550 and 600 K
13 (~ 22 km). At the altitude levels examined here, the largest amount of inferred loss
14 occurred during the 94/95, 95/96, and 99/00 winters and was ~ 2.4 -2.8 ppmv. The
15 inferred loss is compared to simulated loss in the SLIMCAT Chemical Transport
16 Model (CTM). SLIMCAT is able to reproduce the interannual variability observed in
17 the Arctic, but has difficulty reproducing the magnitude of maximum loss. The
18 largest discrepancy corresponds to the cold 94/95 winter, where the model
19 underestimates the loss by ~1 ppmv. SLIMCAT overestimates the loss in 04/05 by
20 0.3-0.4 ppmv; this is the only cold winter for which the loss is overestimated. While
21 this study shows improved agreement between the CTM and observations compared
22 to previous studies, there still remain differences between inferred and modeled ozone
23 loss.

1. Introduction

Meteorological conditions in the Arctic vary substantially from year to year [e.g., *WMO*, 2003; 2006], leading to significant variations in the amount of Arctic O₃ loss [e.g., *Pawson and Naujokat*, 1999; *Manney et al.*, 2003; *Rex et al.*, 2004; *Tilmes et al.*, 2003; 2004]. In order to gain a proper understanding of Arctic O₃ loss, it is thus necessary to examine many winters with different meteorological conditions. To explore the interannual variability in Arctic O₃ loss, we have inferred O₃ loss from satellite observations from the 1994-1995 through the 2004-2005 Arctic winters. Data from both solar occultation and microwave limb sounding instruments are used in this study. These instruments include the Upper Atmosphere Research Satellite Microwave Limb Sounder (UARS MLS), Earth Observing System Microwave Limb Sounder (EOS MLS), Polar Ozone and Aerosol Measurement (POAM II/III), Stratospheric Aerosol and Gas Experiment (SAGE II/III), Improved Limb Atmospheric Spectrometer (ILAS), Halogen Occultation Experiment (HALOE), Atmospheric Chemistry Experiment Fourier Transform Spectrometer (ACE-FTS), and Measurement of Aerosol Extinction in the Stratosphere and Troposphere Retrieved by Occultation (MAESTRO). Since the majority of these instruments did not consistently sample the Arctic vortex throughout the duration of the winter, we have combined the data sets to make one merged O₃ field for each winter. In order to infer O₃ loss from the combined O₃ field, the Chemical Transport Model Passive Subtraction (CTM-PS) technique was applied [e.g., *Deniel et al.* 1998; *Goutail et al.*, 1999; *Guirlet et al.*, 2000; *Sinnhuber et al.*, 2000; *Hoppel et al.*, 2002; *Singleton et al.*, 2005; 2007]. The CTM-PS technique has been adapted from the

well-validated Passive Subtraction approach [e.g., *Manney et al.* 1995 a, b; 1997; 2003; *Harris et al.*, 2002], which was first developed by *Manney et al.* 1995 a, b.

Because the meteorological conditions and the amount of O₃ loss in the Arctic vary from year to year [e.g., *Manney et al.*, 2003; *Tilmes et al.*, 2003], Arctic O₃ loss is much more difficult to simulate than Antarctic processes. To adequately validate the ability of a model to simulate Arctic O₃ loss, modeled O₃ loss must be evaluated during numerous winters that span the range of meteorological conditions. We present modeled Arctic O₃ loss results from the University of Leeds SLIMCAT CTM. The results are then compared to the inferred O₃ loss calculations to determine how well the SLIMCAT CTM was able to simulate Arctic O₃ loss during ten Arctic winters. In addition, the simulated O₃ (as opposed to the ozone loss) is compared to the O₃ observations. Although previous studies have indicated that CTMs underestimate Arctic chemical loss [e.g., *Chipperfield et al.*, 1996; *Goutail et al.*, 1997; *Deniel et al.*, 1998; *Becker et al.*, 2000; *Guirlet et al.*, 2000], adjustments have been made to the SLIMCAT CTM to improve polar O₃ loss processes in the model [*Davies et al.*, 2002; *Feng et al.*, 2005; *Chipperfield*, 2006]. Here we show that these adjustments lead to much better agreement between the model and observations than previously found. Since chemistry modules developed for CTMs are often employed in Chemistry Climate Models, it is vital that CTMs accurately simulate O₃ loss during winters with varying meteorological conditions.

An outline of the paper is as follows. Section 2 describes the satellite ozone data used in this study. Section 3 presents the CTM-PS technique and a discussion of the SLIMCAT model. Section 4 describes the meteorology during the ten Arctic winters analysed here. Section 5 presents the inferred ozone loss results based on the CTM-PS

technique. Section 6 compares the inferred ozone loss using the CTM-PS technique to other methods used to calculate ozone loss. Modeled ozone loss calculations are shown in Section 7. Section 8 compares inferred to modeled ozone loss and discusses possible reasons for discrepancies. Conclusions are presented in Section 9.

2. Satellite ozone data

2.1 POAM II/III

The Polar Ozone and Aerosol Measurement (POAM) instruments, POAM II [Glaccum *et al.*, 1996] and POAM III [Lucke *et al.*, 1999], were nine-channel photometers. The instruments were designed to study chemistry in the polar regions and measure vertical profiles of O₃ and other important stratospheric chemical species. The O₃ observations have a vertical resolution of approximately 1 km in the stratosphere [e.g., Bevilacqua *et al.*, 1997; Randall *et al.*, 2003]. POAM II was launched on the Satellite Pour l'Observation de la Terre (SPOT) 3 satellite in September 1993 and successfully made observations until November 1996 when the satellite failed [Lucke *et al.*, 1999]. SPOT 3 was launched into a sun-synchronous near-polar orbit (98.7° inclination) at an altitude of 833 km, which allowed for approximately 14-15 observations around a circle of latitude in each hemisphere each day [Randall *et al.*, 1995]. The measurement latitude varied slowly between 54° N and 71° N in the Northern Hemisphere, and during the Arctic winter the instrument sampled both inside and outside the polar vortex. POAM II wavelength channels range from .352 to 1.06 μm. For this analysis POAM II version 6.0 O₃ data are used. Rusch *et al.* [1997] showed that an earlier version of the POAM II data

agreed with correlative measurements to within 5-7%, with a low bias below 22 km that reached 20% at 15 km; version 6.0 comparisons are similar.

POAM III was launched in March 1998 on the SPOT 4 satellite; the instrument ceased operations in December of 2005 due to an instrument anomaly. POAM III was launched into the same orbit as POAM II, so its measurement locations are similar to those from POAM II [Lucke *et al.*, 1999]. POAM III channels were slightly different than POAM II, ranging from 0.353 to 1.02 μm . For this analysis POAM III version 4.0 data are used. Randall *et al.* [2003] show that version 3.0 POAM III O₃ measurements agree to within $\pm 5\%$ with correlative ozonesonde and satellite data between 13 and 60 km; version 4.0 comparisons are similar.

2.2 SAGE II/III

The Stratospheric Aerosol and Gas Experiment (SAGE) II first started taking atmospheric observations in October 1984, and ceased operating in August 2005. SAGE II was launched into a 57° mid-inclination orbit aboard the Earth Radiation Budget Satellite (ERBS). Because of its orbit, SAGE II alternated from approximately 60° in the winter hemisphere to 80° in the summer hemisphere in one month, so coverage is temporally sparse in the polar regions, particularly during winter [Wang *et al.*, 2002]. SAGE II utilized solar occultation to measure vertical profiles of O₃ and other stratospheric constituents. SAGE II channels ranged between 0.385 and 1.02 μm . Here we use version 6.2 O₃ data, which varies on the order of 0.5% from version 6.1. Version 6.1 O₃ data agrees within 10% with ozonesondes down to the tropopause, as shown by Wang *et al.* [2002] and has a vertical resolution of approximately 1 km.

SAGE III was launched in December 2001 on the Meteor 3M spacecraft. SAGE III began taking measurements in February 2002 and operations were terminated in March 2006. Like SAGE II, SAGE III also utilized solar occultation [Chu *et al.*, 2002; Thomason and Taha, 2003; Wang *et al.*, 2006]. Unlike SAGE II, SAGE III was launched into a sun-synchronous polar orbit and its Northern Hemisphere observations ranged between 50° and 80° N. The increased northern latitude coverage by SAGE III allows for more detailed Northern Hemisphere polar studies. The spectral coverage for SAGE III ranged between 0.290 and 1.03 μm . SAGE III sampled O₃ with ~ 0.5 km vertical resolution. SAGE III version 3.0 data are applied in this work; these data agree to within 5% with correlative measurements down to 17 km [Wang *et al.*, 2006].

2.3 ILAS

The Improved Limb Atmospheric Spectrometer (ILAS) began taking observations in November 1996 and ceased observations in June 1997 [Sasano *et al.*, 1999]. ILAS consists of an IR spectrometer that operated between 6.21 and 11.76 μm to measure vertical profiles of O₃, as well as other stratospheric species. The vertical resolution of each retrieved species was approximately 1.6 km [Nakajima *et al.*, 2002]. ILAS was launched into a sun synchronous orbit, with a 98.6 ° inclination; it made measurements between 57°N and 72°N in the Northern Hemisphere [Nakajima *et al.*, 2002]. The data applied in this analysis was ILAS version 6.10 [Sugita *et al.*, 2005; Nakajima *et al.*, 2006].

2.4 HALOE

The Halogen Occultation experiment (HALOE) started taking observations in October 1991 and ceased observations in November 2005. HALOE was launched into a mid-inclination orbit (57°) onboard the Upper Atmosphere Research Satellite (UARS) [Reber, 1993]. HALOE used solar occultation to measure absorption bands of many species in the infrared between 2.45 and 10.04 μm , including O_3 [Russell *et al.*, 1993]. Similar to SAGE II, in approximately one month HALOE covered latitudes from about 60° latitude in the winter hemisphere to about 80° latitude in the summer hemisphere. The O_3 vertical resolution is approximately 2 km [e.g., Russell *et al.*, 1993; Randall *et al.*, 2003]. HALOE version 19 data was used in this analysis. This version has been compared with an earlier version of SAGE II data (6.0) by Morris *et al.* [2002], who indicate that differences between the datasets varied from 4–12% throughout most of the stratosphere.

2.5 ACE-FTS and MAESTRO

The Atmospheric Chemistry Experiment Fourier Transform Spectrometer (ACE-FTS) and the Measurement of Aerosol Extinction in the Stratosphere and Troposphere Retrieved by Occultation (MAESTRO) instruments were launched onboard the ACE satellite in August 2003 and are currently operational. Both instruments utilize solar occultation. The ACE spacecraft was launched into a high inclination orbit (74°). The solar occultation sampling is thus similar to SAGE II and HALOE in that a broad range of latitudes is covered in about a month, but substantial time is spent at high latitudes. ACE-FTS operates in the 2 to 13 micron spectral region and measures many constituents, including O_3 , at a vertical resolution of approximately 4 km in the lower stratosphere [Bernath *et al.*, 2005]. ACE-FTS version 2.2 O_3 update was used for this analysis, which

has improved agreement with correlative observations near the profile peak compared to versions 1.0 and 2.2. MAESTRO makes observations in the 400 to 1030 nm spectral region. MAESTRO measures vertical profiles of O₃, NO₂, and aerosol extinction with a vertical resolution of approximately 1 km. We use version 1.2 MAESTRO data for this analysis. *Kar et al.* [2007] show that v1.2 MAESTRO O₃ profiles agree with correlative measurements from ACE-FTS, SAGE III, and POAM III to within about 15% in the lower stratosphere.

2.6 UARS/EOS MLS

Data was analyzed from two microwave limb sounding instruments in this study, the Upper Atmosphere Research Satellite Microwave Limb Sounder (UARS MLS) [*Barath et al.*, 1993] and the Earth Observing System Microwave Limb Sounder (EOS MLS) [*Waters et al.*, 2006]. The mid-inclination UARS orbit allowed the UARS MLS instrument to take measurements from latitudes of approximately 34° on one side of the equator to 80° on the other. Approximately every 36 days UARS performed a yaw maneuver and switched viewing orientation by 180° degrees. Because of the yaw cycle, UARS MLS coverage of the high northern latitudes was limited during the winter. UARS MLS measured emission spectra near 63, 205, and 183 GHz using three radiometers [*Livesey et al.*, 2003]. UARS MLS started taking observations in September 1991 and continued operating at a full level of operation until December 1993. After this time, measurement coverage started to become more intermittent, until the instrument was decommissioned in December 2005. UARS MLS data version 5, which has been validated by *Livesey et al.* [2003], was applied in this analysis. *Livesey et al.* [2003] state

that agreement with SAGE II O₃ is typically within 5%; however, larger differences (~30%) are observed at low latitudes (30°S- 30°N). O₃ has a vertical resolution of approximately 3.5 – 4 km in the lower stratosphere [Manney *et al.*, 2003].

EOS MLS was launched in July 2004 onboard the Aura satellite. Aura is in a near-polar, sun-synchronous orbit; thus EOS MLS observations span from 82° S to 82° N on every orbit [Waters *et al.*, 2006]. As a result of the orbit, EOS MLS samples the northern polar latitudes more continuously throughout the winter than UARS MLS. EOS MLS has 5 radiometers that operate in the following spectral regions: 118 GHz, 190 GHz, 240 GHz, 640 GHz, and 2.5 THz [Waters *et al.*, 2006]. In the lower stratosphere the vertical resolution for O₃ is approximately 2.7 km [Froidevaux *et al.*, 2006]. The MLS data applied in this study is version 1.51, which has been validated by Froidevaux *et al.* [2006]. Froidevaux *et al.* [2006] found that the overall agreement between EOS MLS O₃ and stratospheric profiles from SAGE II, HALOE, POAM III, and ACE-FTS was approximately 5% to 10%.

3. Methods

The CTM-Passive Subtraction (CTM-PS) technique was applied to infer O₃ loss from both solar occultation and limb emission observations. The CTM-PS technique was developed from the passive subtraction technique, which was first described by Manney *et al.* [1995a, b, 2003], and has since been applied in many O₃ loss studies [e.g., Deniel *et al.*, 1998; Singleton *et al.*, 2005; 2007]. In order to infer O₃ loss from observations, the CTM-PS technique requires that a passive O₃ field (i.e., globally distributed O₃ profiles

that are assumed to vary only because of dynamics, not chemistry) be generated by a CTM. The passive O₃ field is then interpolated to the measurement locations and the difference between the observations and the passive field is the inferred O₃ loss (IL). The passive O₃ field can also be subtracted from the “active” model O₃ field (referred to here as the modeled or simulated O₃), in which both the chemistry and dynamics are activated, to quantify the modeled O₃ loss (ML). For the work described here, the ML was computed at the observation locations in order to be directly compared with the IL calculations.

The University of Leeds SLIMCAT CTM was used for this analysis. SLIMCAT is a 3-D offline model with detailed stratospheric chemistry, which includes heterogeneous chemistry on solid and liquid aerosols and a NAT-based denitrification scheme (see *Davies et al.* [2002]). The model is described in detail by *Chipperfield* [1999] and recent adjustments to the model are discussed by *Feng et al.* [2005; 2007a] and *Chipperfield* [2006]. The vertical domain of the model extends from the surface to approximately 55 km. The vertical grid in SLIMCAT is a hybrid sigma-theta grid, which is described in *Chipperfield* [2006], and has isentropic coordinates in the stratosphere above 350 K. The vertical resolution in the stratosphere is approximately 2 km, comparable to remote sensing observations. For the runs used in this study, SLIMCAT was forced with daily temperatures and horizontal winds from the European Centre for Medium-Range Weather Forecasts (ECMWF) analyses. Runs prior to 1 January 2000 were forced with the re-analyses (ERA-40), and runs after this date were forced with the operational analyses. The ERA-40 temperatures have a slight bias compared to those in other meteorological analyses; nevertheless, studies have shown that ERA-40 correctly

handles interannual variability [e.g., *Manney et al.*, 2005; *Tilmes et al.*, 2006]. However, vertical oscillations in ERA-40 temperatures have been shown to impact model chlorine activation and O₃ loss in CTMs [e.g. *Feng et al.*, 2005]. The vertical transport in the stratosphere is based on calculations from the NCAR CCM radiation scheme [*Briegleb*, 1992].

Prior to the winter simulations, a low resolution (7.5 x 7.5°) run was started on 1 January 1977. The results of this run were then used to initialize the high resolution (2.8 x 2.8°) model runs on 1 December of each year from 1994 to 2004. The only exceptions were for the 2002-2003 and 1999-2000 runs, where the modeled O₃ was initialized from O₃ fields constructed from Northern Hemisphere observations from POAM III and HALOE using PV-mapping, as described in *Randall et al.* [2002, 2005] (see *Singleton et al.* [2005]). The impact of the model O₃ initialization will be discussed in more detail in Section 5. The model runs presented here have the same setup as those described in *Feng et al.* [2005, 2007b] and *Chipperfield et al.* [2005]. The tropospheric source gases in SLIMCAT are based on *WMO* [2003] values. The only additional difference between the model runs analyzed here is the bromine loading for the 2004-2005 run. The 2004-2005 simulation includes an extra 6 pptv of lower stratospheric Br_y from short-lived species, which is based on the findings of *Salawitch et al.* [2005]. This change is not expected to have an impact on the short-term winter simulations, but would have an impact on the mid-latitude O₃ trend for a long-term run [*Feng et al.*, 2007a].

Throughout the 1994-1995 through the 2004-2005 Arctic winters (defined here as the time period from 1 December – 1 April), there was a wealth of stratospheric observations from solar occultation and microwave limb sounding instruments, although

not all of the instruments made observations throughout the duration of each winter. To illustrate this point, Figure 1 shows the equivalent latitude of all vortex observations. Equivalent latitude is a vortex-centered coordinate system, where 90° is always at the center of the vortex [Butchart and Remsberg, 1986]. The equivalent latitude was calculated from Met Office (MetO) Potential Vorticity (PV) at the MetO model grid and then was interpolated to the observation locations. The only year that will not be discussed in this paper is the 1997-1998 winter, because there were so few vortex observations made during this winter (as indicated by Figure 1). There were only slightly more vortex observations during the 2000-2001 winter; therefore, the O_3 loss results computed for this winter will only be discussed qualitatively.

In previous studies by Singleton *et al.* [2005; 2007], inferred loss (IL) and modeled loss (ML) calculations were computed separately for each instrument during the Arctic winters of 2002-2003 and 2004-2005. In order to utilize all of the datasets in the current study, the O_3 observations were combined to make one O_3 field for each winter. To do so, all the instruments were normalized to eliminate offsets in the O_3 field due to individual instrument biases. Because SAGE II was one of the only instruments that made observations throughout the 1994-1995 through 2004-2005 time period, all instruments were corrected to SAGE II using different normalization factors.

For all instruments except UARS and EOS MLS, comparisons between coincident measurements that were within 2 hours and 500 km were used to determine the normalization factor. In order to find an adequate number of coincidences with the MLS instruments, which did not typically measure at sunrise and sunset, the time criterion was extended to 12 hours. The average ratio of SAGE II to the coincident

profiles was used to normalize the measurements to SAGE II at each altitude. Figure 2 shows the normalization profiles that were applied to each instrument. The normalization profiles indicate that the differences between the instruments are well within 20%. The only exception is for UARS MLS, which has differences that are greater than 50% below 425 K, which is below the altitude levels validated by *Livesey et al.* [2003]. Therefore, UARS MLS data below 425 K have not been included in the analyses. Once the satellite datasets were normalized, all vortex observations were combined for each winter. The SLIMCAT (passive and modeled) O₃ was then sampled at each observation location. In order to determine the vortex edge, the vortex definition of *Harvey et al.* [2002] was applied. IL and ML calculations were computed between 400 and 700 K for observations inside the vortex. The calculations were not extended below 400 K due to uncertainties in identifying the vortex edge (see *Singleton et al.* [2007] for additional details).

4. Meteorology

Due to the large variability in meteorological conditions in the Arctic winter, the formation of polar stratospheric clouds (PSCs) varies each year [e.g., *Pawson et al.*, 1995; *Pawson and Naujokat*, 1999; *Massoli et al.*, 2006]. During cold winters, Arctic temperatures are more likely to drop below those at which nitric acid trihydrate (NAT) can condense (T_{NAT}) resulting in a larger occurrence of PSCs. The area in the Northern Hemisphere where winter temperatures fell below T_{NAT} is shown in Figure 3 for all winters from 1994-1995 through 2004-2005. T_{NAT} values were computed using the expression from *Hanson and Mauersberger* [1988] using SLIMCAT HNO₃ and H₂O and MetO temperature analyses. Figure 3 indicates that the 1995-1996, 1999-2000, and

2004-2005 winters had the largest areas with $T < T_{\text{NAT}}$. The warmest winter was the 1998-1999 winter, which only had two short periods, in early December and February, where temperatures fell below T_{NAT} .

Another important diagnostic of the meteorological conditions is the strength of the polar vortex. Unlike the Antarctic vortex, which is almost always cold and stable, the Arctic vortex is continuously disturbed by planetary waves that propagate up from the troposphere [e.g., Charney and Drazin, 1961]. When the Arctic vortex is disturbed, mixing is more likely to occur across the vortex edge, which can complicate O_3 loss calculations [e.g., Plumb *et al.*, 2000; Harris *et al.*, 2002; Müller *et al.*, 2005]. In order to assess the strength of the Arctic vortex and the timing of potential mixing events during the years included in the climatology, we define a diagnostic for vortex strength as the average wind speed at the vortex edge multiplied by a normalized PV gradient. This normalized PV gradient is defined by the ratio of the PV gradient at any location to the maximum value of the PV gradient, resulting in a unitless index ranging from 0 to 1. This vortex strength diagnostic is shown in Figure 4 for the years 1994-1995 through 2004-2005 as a function of altitude and time. If the maximum PV gradient is exactly collocated with the polar jet, then this diagnostic is reduced to the average wind speed at the vortex edge. If the maximum PV gradient is not collocated with the jet then the magnitude of this diagnostic decreases. A high vortex strength index indicates that the polar night jet is strong and the flow is aligned with steep PV gradients. In this situation, air is more likely to be confined within the vortex and not mix with extra-vortex air.

Figure 4 indicates that there was a large amount of variability in the strength of the vortex during the Arctic winters. The winters that are characterized by a strong

vortex in the altitude region of interest here (~400-700 K) from December through March are the 1994-1995, 1995-1996, and 1999-2000 winters; combined with the low temperatures described above, these winters had the highest potential for significant O₃ loss. The 2004-2005 winter had a high vortex strength index through February, but a major final warming early in March [Manney *et al.*, 2006] drastically decreased the polar night jet speed. The vortex was relatively weak at the beginning of the 1996-1997 winter, but strengthened considerably in January and remained strong for the rest of the winter. The winters of 1998-1999 and 2000-2001 are characterized by the weakest vortex of the years investigated, followed by 2001-2002 and 1997-1998. Both the 2002-2003 and the 2003-2004 winters experienced major warmings in January [Manney *et al.*, 2005]. The 2002-2003 vortex was able to regain some strength after the warming; however, the 2003-2004 vortex remained weak and warm in the lower stratosphere, reducing the potential for large O₃ losses.

Both the vortex strength and temperature indicate potential for O₃ loss. On the basis of these two factors alone, and considering only the overall behavior throughout the winter, the expectation is that O₃ loss potential, at the altitude levels examined in this study, would be large for 1994-1995, 1995-1996, 1999-2000; moderate for 1996-1997, 2002-2003, 2004-2005; and low for 1998-1999, 2000-2001, 2001-2002, and 2003-2004. Note that moderate loss would be expected for 1997-1998, but as noted above, too few observations were available for O₃ loss quantification that winter. There are of course other factors, in addition to the ones described above, which can influence the amount of O₃ loss during a given winter (e.g. vortex position, vortex shape, and concentricity of the

vortex and cold region). These factors can vary substantially from year to year resulting in a potential for large annual variability in Arctic O₃ loss.

5. Inferred Loss

The daily averaged IL inside the vortex for the ten Arctic winters analyzed here is shown in Figure 5. As mentioned above, the IL is the difference between the observed O₃ field and the passive O₃ interpolated to the observation locations. For qualitative purposes, data void regions on days when a vortex observation was not made have been interpolated in time. In addition, data in all of the contour plots have been smoothed using a seven-day running average.

Singleton et al. [2005; 2007] discuss the importance of model initialization when applying the CTM-PS technique to calculate O₃ loss. In order to correctly infer O₃ loss from the observations, it is necessary that the passive O₃ is equal to the observations on the first day of the analysis (1 December). If there are any differences between the passive O₃ and the observations at the start of the analysis, the differences will be propagated in the passive O₃. Consequently, these differences can affect the IL calculations at a later date in the analysis. For example, a negative offset on the first day of the analysis would falsely indicate that chemical loss had occurred [*Singleton et al.*, 2005; 2007]. In this analysis, the model passive O₃ was not initialized with the combined O₃ fields, so there is an offset on 1 December in some of the years. In order to correct for this offset, the model passive O₃ field has been corrected to account for any initialization differences. This was accomplished by adjusting the modeled O₃ by a correction profile equal to the average difference between the observed ozone and the simulated ozone

during the first 9 days of December. The same correction profile has been applied to the model active O₃, since the passive and the active O₃ are equal on 1 December.

As previously mentioned, since there is large interannual variability in the meteorological conditions in the Arctic, the amount of O₃ loss changes from year to year. This interannual variability is evident in Figure 5. It is important to note that the smoothness of the contours varies with the number of observations that were included in the average. For example, during the 2004-2005 winter, observations from seven satellite instruments (including EOS MLS) were used in the average, compared to just three during the 2001-2002 winter (see Figure 1). There were very few observations taken during the 2000-2001 winter; therefore, conclusive statements will not be made about this winter. To examine the IL in a more quantitative manner, a time series of the daily average IL is shown in Figure 6 for the 600, 500, 475, and 450 K surfaces. Days when vortex observations were not made have not been interpolated in the time series figures.

The CTM-PS technique indicates that within the altitude levels examined here (400 to 700 K), the largest amount of loss occurred during the 1994-1995, 1995-1996, and 1999-2000 winters. As mentioned above, these winters experienced extended periods of very low temperatures ($T < T_{\text{NAT}}$) and had strong polar vortices. As a result, these winters had the highest potential for significant O₃ loss of the ten winters analyzed here. The maximum loss for these cold winters occurred between 450 and 500 K and ranged from approximately 2.4-2.8 ppmv.

The winter of 2004-2005 experienced somewhat less loss, with a maximum of ~1.8 ppmv between 450 and 500 K. The limited loss may be due to the early final warming mentioned above, and dynamical activity that resulted in mixing of extra-vortex

air into the vortex [Manney *et al.*, 2006; Schoeberl *et al.*, 2006]. Even though the 2004-2005 winter experienced very low temperatures (similar to 1999-2000), the mixing would likely have limited the amount of O₃ loss at some altitudes during the winter [Manney *et al.*, 2006; Von Hobe *et al.*, 2006]. As expected from the temperatures and vortex index, the 2002-2003 and 1996-1997 winters also had a moderate amount of loss, with maximum loss of about 1.5 ppmv. The 2002-2003 winter had a maximum loss near 450 K, while the peak loss in the 1996-1997 winter spanned a much broader altitude region between 450 K and 550 K.

Contrary to expectations based only on the overall vortex strength and temperature, the 2001-2002 and 2003-2004 winters also had a moderate amount of loss, around 1.7 to 2 ppmv. Both winters had similar morphology, and experienced more loss above 550 K than the other winters. The peak O₃ loss for 2001-2002 and 2003-2004 occurred between approximately 575 and 600 K. Both of these winters had areas where temperatures were below T_{NAT} at the beginning of the winter at the higher potential temperature levels, but not later in the winter at lower altitudes. In other words, PSCs probably formed efficiently only in the upper altitudes, which led to loss in those regions, but not below.

Of all the winters examined here, the 1998-1999 winter experienced the least amount of O₃ loss. This winter was much warmer than the other winters and had a very unstable vortex. A maximum loss of approximately 0.9 ppmv occurred near 550 K. The 2000-2001 winter also experienced minimal loss; however, because so few observations were made during this winter conclusive statements cannot be made about the O₃ loss.

Overall, maximum O₃ loss occurred between 400 and 500 K in most years; however, for three of the years (1998-1999, 2001-2002, and 2003-2004) maximum O₃ loss occurred at higher altitudes (550 – 600 K). Figure 6 also indicates there is a positive slope primarily in the differences at 600 K between the observations and modeled passive O₃ during December. O₃ mixing ratios are generally greater outside the vortex than inside at this level due to poleward transport of O₃ rich subtropical air [*Manney et al.*, 1995; *Randall et al.*, 1995; *Singleton et al.*, 2005]. These results are similar to those presented in *Singleton et al.* [2007], and can likely be attributed to horizontal transport that is not captured by the model.

6. Comparison with Other Techniques

In this section CTM-PS IL during the winters with the largest O₃ loss (1994-1995, 1995-1996, and 1999-2000) is compared to inferred loss which has been computed using other well validated O₃ loss techniques. Each study was run for different time periods during the winter and with different datasets; therefore, some differences are expected between the calculations.

The CTM-PS IL results for the 1994-1995 winter are comparable to the results of *Rex et al.* [1999]. *Rex et al.* [1999] applied the Match technique using ozonesonde observations to calculate a cumulative loss at 450 K of 2.0 ppmv. These loss results are slightly lower than the 2.4 - 2.7 ppmv loss computed by CTM-PS in late March at 450 K. However, the differences can be attributed to the time duration of the analyses. *Rex et al.* [1999] computed the cumulative O₃ loss from 1 January through 20 March and the CTM-

PS analysis was started on 1 December. By 1 January, 0.35 ppmv of O₃ loss had already occurred in the CTM-PS results.

For the 1995-1996 winter, the CTM-PS technique indicates that a maximum loss of approximately 2.1 to 2.4 ppmv occurred at 450 K. These results are comparable to the results of *Rex et al.* [1997] and *Müller et al.* [1997]. *Rex et al.* [1997] applied the Match technique to ozonesonde observations and found a maximum cumulative loss of approximately 2.4 ppmv between 20 January and 9 April. *Müller et al.* [1997] inferred O₃ loss from HALOE observations using the O₃-tracer technique. The results indicate that the peak loss during the 1995-1996 winter occurred near 450 K and was approximately 3.3 ppmv. Differences between CTM-PS and *Müller et al.* [1997] are likely due to sampling of the instruments. The combined satellite O₃ fields (and ozonesonde data) are more representative of vortex-average conditions compared to using data from just one satellite instrument. In addition, differences may be attributed to the large uncertainties inherent in the O₃-tracer technique when determining an accurate initialization relation.

The CTM-PS IL results indicate absolute maximum O₃ loss between 2.4 and 2.8 ppmv at 450 K during the 1999-2000 winter. These results are larger than the maximum loss calculated by *Hoppel et al.* [2002] using the vortex average approach with POAM III data. *Hoppel et al.* [2002] found the maximum loss occurred near 475 K and was approximately 1.5-2 ppmv during this winter. However, *Hoppel et al.* [2002] only computed the loss until 15 March; by 15 March the CTM-PS IL is on the order of 2.2 ppmv at 450-475 K.

While there are differences between the results for each of the techniques, overall the comparisons for the 1994-1995, 1995-1996, and 1999-2000 winters are in good agreement.

7. Modeled Loss (ML)

The daily average vortex ML for the ten Arctic winters is shown in Figure 7. The model has been sampled at the different instrument locations and then combined as was done with the IL calculations. Figure 7 shows that in most winters, SLIMCAT is able to reproduce the general pattern of the IL shown in Figure 5. The vertical region of maximum loss in SLIMCAT is generally the same as in the observations. In every winter except 2004-2005, however, the model shows less loss than is inferred from the observations. During 2004-2005 SLIMCAT slightly overestimates the maximum loss near 450 K because the model overestimated chlorine activation (not shown). The same result was found by *Singleton et al.* [2007] where the loss was inferred separately from the POAM III, SAGE III, EOS MLS, MAESTRO, and ACE-FTS instruments.

The time series of the ML and scatter plots of the ML and IL are shown in Figures 8 and 9, respectively. Figure 8 indicates that there is much less variability in the ML compared to the IL results; this is particularly true at 600 K. At this altitude, the model is unable to capture the maximum loss for the 2001-2002 and 2003-2004 winters. For both of these winters, SLIMCAT underestimates O₃ loss by approximately 1 ppmv.

Figure 9 shows that below 600 K SLIMCAT has difficulty simulating the maximum O₃ loss during the cold 1994-1995 and the 1995-1996 winters. Conversely, SLIMCAT slightly overestimates the loss during 2004-2005 on the 475 K and 450 K

surfaces. At these levels SLIMCAT indicates that the 2004-2005 winter had the largest amount of loss of all the winters, and overestimates the loss compared to the IL by approximately 0.3-0.4 ppmv. Although there were some discrepancies between the IL and ML results during the 1994-1995, 1995-1996, and 2004-2005 winters, SLIMCAT had less difficulty simulating the maximum loss for the cold 1999-2000 winter below 500 K.

The extent of agreement between the maximum IL and ML results at the end of the analysis time period is shown for each year in Figure 10. The top panel is a time series of the average maximum IL (black) and ML (red) over the last 14 days of the analysis for the ten Arctic winters. The bottom panel of Figure 10 shows the altitude at which the maximum loss occurred. The figure indicates that although there are some differences in the magnitude and the location of the maximum loss, overall SLIMCAT is able to capture the interannual variability observed in the Arctic quite well. Specifically, the model did show that the peak loss during warm winters (1998-1999, 2001-2002, and 2003-2004) occurred at higher altitudes. As mentioned above, the maximum loss in the observations occurred during the 1994-1995, 1995-1996, and 1999-2000 winters. These were the winters with low temperatures ($T < T_{\text{NAT}}$) and prolonged periods of high vortex strength index. For these years the average loss was approximately 2.4 ppmv. The model indicated that the maximum loss occurred during the 2004-2005 winter, the year with maximum PSC formation probability, at approximately 2.2 ppmv. However, the 1995-1996 and 1999-2000 winters also had a large amount of loss around 2 ppmv.

Figure 11 shows the average O_3 loss for the last 14 days of the analysis on the 450 K and 600 K potential temperature surfaces. We chose these levels because maximum

loss tends to occur at the lower altitudes near 450 K in cold years, whereas maximum loss tends to occur at the higher altitudes during warm years. The ML and IL agree very well at 450 K, but much more poorly at 600 K. The largest discrepancy at 450 K occurs during the cold 1994-1995 winter, when the model underestimates the loss by approximately 1 ppmv. In all other winters, both warm and cold, the agreement at 450 K between the ML and IL is excellent, although there is a clear tendency for the model to underestimate the loss compared to the observations, as discussed above. The level of agreement at 600 K is not as satisfying, with the model underestimating the loss compared to the IL in both 2001-2002 and 2003-2004 by 0.8-1.0 ppmv. It is likely that the IL in these two warm winters resulted from heterogeneous chemistry that occurred early in the winter when the T_{NAT} area was relatively small but centered at higher altitudes. This suggests that heterogeneous processing at the higher altitudes is not handled correctly by the model.

8. Observed and Simulated O_3

The differences between the IL and the ML are due to differences between the observed and simulated O_3 itself (since both rely on the same model passive O_3). These differences may be caused by an error in the chemistry and/or dynamics in the model. The daily average O_3 for the ten Arctic winters is shown for the observations and the modeled O_3 in Figures 12 and 13, respectively. The differences between the model and the observations (Figure 13 minus Figure 12) are shown in Figure 14. Overall, the similarities between the model and observations are remarkable. This is true for the large scale features such as the relatively larger O_3 mixing ratios in 1998-1999 compared to

other years and the temporal variation in low O₃ mixing ratios each year below 500 K. At 600 K and below, dynamical effects and chemistry that occurs after chlorine activation on polar stratospheric clouds can alter vortex O₃ values. At 600 K the largest differences between the observations and the modeled O₃ took place during the 2001-2002 and 2003-2004 winters, when SLIMCAT overestimated the amount of O₃. As a result, the model underestimated the maximum loss observed during these winters (as shown in the right panel of Figure 11). At 600 K, O₃ mixing ratios are generally larger outside the vortex; therefore, vortex O₃ will be increased if mixing with extra-vortex air occurs. As mentioned above, the 2001-2002 and 2003-2004 winters were both dynamically active and experienced extended periods where the vortex was disturbed (see Figure 4). Therefore, the discrepancies between the observations and the modeled O₃ during those years are likely the result of the model overestimating the amount of mixing that took place due to the coarse horizontal resolution of the CTM.

During cold winters, with the exception of the 2004-2005 winter, the model overestimates O₃ at 450 K, which results in an underestimation of ML. Similar to the 600 K level, mixing with extra-vortex air at 450 K can lead to changes in O₃. At 450 K O₃ mixing ratios are generally smaller outside the vortex than inside; therefore, mixing of extra-vortex air into the vortex would give the appearance of chemical loss. At 450 K, the largest differences between the observations and the modeled O₃ occur during the 1994-1995 winter, where the model overestimates the amount of O₃. This overestimation results in too little ML (as shown in the left panel of Figure 11). During February 1995 the vortex was displaced to lower latitudes due to a minor warming [e.g., *Naujokat et al.*, 1995; *Müller et al.*, 1996]. However, the vortex was not as disturbed as in other years, so

it is unclear why there is such a large difference between the observations and the model O_3 during this year.

The 2004-2005 winter was the only cold winter in which SLIMCAT underestimates the O_3 at 450 K in March, which corresponds to the overestimation of ML. *Manney et al.* [2006] indicate that EOS MLS N_2O observations confirm that mixing was occurring during this time, so it is likely that the model was too diffusive in the lower stratosphere.

9. Conclusions

More so than in the Antarctic, Arctic ozone loss undergoes large interannual variability due to the changing dynamics and meteorological conditions. In order to explore the interannual variability, we have presented a climatology of O_3 loss during ten Arctic winters using the chemical transport model (CTM) Passive Subtraction technique. O_3 loss calculations were inferred from O_3 data fields which were formed from observations made by the UARS MLS, EOS MLS, POAM II/III, SAGE II/III, ILAS, HALOE, ACE-FTS, and MAESTRO instruments. Results indicate that in most years the maximum O_3 loss occurred between 400 and 500 K. However, warmer winters (1998-1999, 2001-2002, and 2003-2004) experienced maximum loss at higher altitudes (550-600 K). Analyses confirm that the most significant O_3 loss occurs when the vortex is strongest. In addition, temperatures must be below T_{NAT} at the same time the vortex is strong and stable. The winters that experienced the largest amount of O_3 loss were 1994-1995, 1995-1996, and 1999-2000. These were also the winters that had the strongest and most extensive (in altitude and time) vortex when considered over the entire season, but

did not necessarily have the largest probability of PSC formation. The average loss during these cold winters was approximately 2.4 ppmv, which was found to be comparable to results from other O₃ loss techniques. Each of these winters had a very strong vortex during periods when the temperature fell below T_{NAT}.

In this study we compared modeled O₃ loss from the 3-D SLIMCAT CTM to loss inferred from observations to determine how well the CTM was able to simulate O₃ loss during the ten Arctic winters with varying meteorological conditions. Overall, the morphology of the modeled O₃ loss was similar to that of the inferred loss during each of the different winters. The winters with a significant amount of loss in the model were 1994-1995, 1995-1996, 1999-2000, and 2004-2005. The largest amount of loss occurred during 2004-2005, for which the average loss during the last 14 days of the analysis was approximately 2.2 ppmv; this was slightly larger than the observations by approximately 0.3-0.4 ppmv. The 2004-2005 winter was the only winter in which SLIMCAT overestimated the maximum observed loss, possibly because of improper treatment of mixing. In every other winter SLIMCAT underestimated the loss. Future work will involve comparing other observations to the model in order to fully test the model's ability to simulate the chemistry and dynamics for each of these ten Arctic winters. Overall, SLIMCAT was able to reproduce the morphology and the interannual variability of O₃ loss inferred from Arctic observations during ten Arctic winters.

This study shows that, while knowledge of polar O₃ loss has progressed since the discoveries of *Farman et al.* [1985], there is still progress that needs to be made in the modeling of stratospheric O₃ loss processes in the Arctic. Stratospheric modeling capabilities have improved since previous studies and results presented here indicate that

the SLIMCAT CTM is able to simulate interannual variability in stratospheric O₃. However, CTMs still have difficulty quantitatively reproducing the maximum loss that is inferred from observations. Since CTMs play an integral part in developing atmospheric chemistry modules in Chemistry Climate Models, improving the agreement between inferred and modeled O₃ loss results is important for reliable predictions of future Arctic O₃ losses.

9. Acknowledgements

This research is supported by the NASA Earth System Science Fellowship and the NASA Solar Occultation Satellite Science Team Program. We would like to thank colleagues at the United Kingdom Meteorological Office for producing the MetO analyses. We thank the ACE, HALOE, ILAS, MLS, POAM, and SAGE instrument science teams for the satellite data. We would also like to thank the Distributed Active Archive Center at the Goddard Space Flight Center and the British Atmospheric Data Centre for distributing the data. ILAS was developed by the Environment Agency of Japan and was on board the ADEOS launched by the National Space Development Agency of Japan. The ILAS data were processed at the ILAS Data Handling Facility, the National Institute for Environmental Studies. ACE is supported by the Canadian Space Agency. Work at the Jet Propulsion Laboratory, California Institute of Technology was done under contract with the National Aeronautics and Space Administration.

10. References

Barath, F.T., et al. (1993), The Upper Atmosphere Research Satellite microwave limb sounder instrument, *J. Geophys. Res.*, *98*, 10,751–10,762.

Becker, G., R. Müller, D.S. McKenna, M. Rex, K. Carslaw, and H. Oelhaf (2000), Ozone loss rates in the Arctic stratosphere in the winter 1994-1995: Model simulations underestimate results of the Match analysis, *J. Geophys. Res.*, *105*, 15,175-15,184.

Bernath, P. F., et al. (2005), Atmospheric Chemistry Experiment (ACE):Mission overview, *Geophys. Res. Lett.*, *32*, L15S01, doi:10.1029/2005GL022386.

Bevilacqua, R. M., et al. (1997), POAM II ozone observations in the Antarctic ozone hole in 1994, 1995, and 1996, *J. Geophys. Res.*, *102*(D19), 23,643–23,658.

Briegleb, B. P. (1992), Delta-Eddington Approximation for Solar Radiation in the NCAR Community Climate Model, *J. Geophys. Res.*, *97*, 7603–7612.

Butchart, N., and E.E. Remsberg (1986), The area of the stratospheric polar vortex as a diagnostic for tracer transport on an isentropic surface, *J. Atmos. Sci.*, *43*, 1319-1339.

Charney, J.P., and P.G. Drazin, (1961), Propagation of planetary-scale disturbances from the lower into the upper atmosphere. *J. Geophys. Res.*, *66*, 83-109.

Chipperfield, M.P., A.M. Lee, and J.A. Pyle (1996), Model calculations of ozone depletion in the Arctic polar vortex for 1991/92 to 1994/95, *Geophys. Res. Lett.*, *23*, 559-562.

Chipperfield, M. P. (1999), Multiannual simulations with a three-dimensional chemical transport model, *J. Geophys. Res.*, *104*, 1781–1805.

Chipperfield, M.P., W. Feng, and M. Rex (2005), Arctic Ozone Loss and Climate Sensitivity: Updated Three-Dimensional Model Study, *Geophys. Res. Lett.*, Vol. 32, No. 11, L11813, 10.1029/2005GL022674.

Chipperfield, M. P. (2006), New version of the TOMCAT/SLIMCAT off-line chemical transport model: Intercomparison of stratospheric tracer experiments, *Q.J.R. Meteorol. Soc.*, *132*, 1179-1203.

Chu, W.P. C.R. Trepte, R.E. Veiga, M.S. Cisewski, and G. Taha (2002), SAGE III measurements, *Proc. SPIE Int. Soc. Opt. Eng.*, *48*, 457-464.

Davies, S., M. P. Chipperfield, K. S. Carslaw, B. M. Sinnhuber, J. G. Anderson, R. M. Stimpfle, D. M. Wilmouth, D. W. Fahey, P. J. Popp, E. C. Richard, P. von der Gathen, H. Jost, and C. R. Webster (2002), Modeling the effect of denitrification on Arctic ozone depletion during winter 1999/2000, *J. Geophys. Res.*, doi:10.1029/2001JD000445.

Deniel, C., R.M. Bevilaqua, J.P. Pommereau, and F. Lefèvre (1998), Arctic chemical ozone depletion during the 1994-1995 winter deduced from POAM II satellite observations and the REPROBUS three-dimensional model, *J. Geophys. Res.*, *103*, 19,231 – 19,244.

Feng, W., M.P. Chipperfield, S. Davies, B. Sen, G. Toon, J.F. Blavier, C.R. Webster, C.M. Volk, A. Ulanovsky, F. Ravagnani, P. von der Gathen, H. Jost, E.C. Richard and H. Claude (2005), Three-Dimensional Model Study of the Arctic Ozone Loss in 2002/03 and Comparison with 1999/2000 and 2003/04, *Atmos. Chem. Phys.*, *5*, 139-152.

Feng, W., M.P. Chipperfield, M. Dorf, K. Pfeilsticker, and P. Ricaud (2007a), Mid-latitude ozone changes: Studies with a 3-D CTM forced by ERA-40 analyses, *Atmos. Chem. Phys.*, *7*, 2357-2369.

Feng W., M.P. Chipperfield, S. Davies, P. von der Gathen, E. Kyro, C.M. Volk, A. Ulanovsky, G. Belyaev (2007b), Large Chemical Ozone Loss in 2004/05 Arctic Winter/Spring, *Geophys. Res. Lett.*, *34*, L09803, doi:10.1029/2006GL029098.

Froidevaux, L., et al. (2006), Early validation analyses of atmospheric profiles from EOS MLS on the Aura satellite, *IEEE Trans. Geosci. Remote Sensing* *44*, no. 5, 1106-1121.

Glaccum, W., et al. (1996), The Polar Ozone and Aerosol Measurement instrument, *J. Geophys. Res.*, *101*(D9), 14,479–14,488.

Goutail, F., N.R.P. Harris, I. Kilbane-Dawe, and G.T. Amanatidis (1997), Ozone loss: the global picture, Proc. European Ozone Meeting, Schliersee, Germany.

Groß, J.-U., et al. (2002), Simulation of ozone depletion in spring 2000 with the Chemical Lagrangian Model of the Stratosphere (CLaMS), *J. Geophys. Res.*, *107*(D20), 8295, doi:10.1029/2001JD000456.

Guirlet, M., M.P. Chipperfield, J.A. Pyle, F. Goutail, J.P. Pommereau, and E. Kyrö (2000), Modeled Arctic ozone depletion in winter 1997/1998 and comparison with previous winters, *J. Geophys. Res.*, *105*, 22,185-22,200.

Hanson, D. and K. Mauersberger (1988), Laboratory studies of the nitric acid trihydrate: Implications for the south polar stratosphere, *Geophys. Res. Lett.*, *15*, 855-858.

Harris, N. R. P., M. Rex, F. Goutail, B. M. Knudsen, G. L. Manney, R. Müller, and P. von der Gathen (2002), Comparison of empirically derived ozone losses in the Arctic vortex, *J. Geophys. Res.*, *107*(D20), 8264, doi:10.1029/2001JD000482.

Harvey, V. L., R. B. Pierce, T. D. Fairlie, and M. H. Hitchman (2002), A climatology of stratospheric polar vortices and anticyclones, *J. Geophys. Res.*, *107*(D20), 4442, doi:10.1029/2001JD001471.

Hoppel, K., R. Bevilacqua, G. Nedoluha, C. Deniel, F. Lefèvre, J. Lumpe, M. Fromm, C. Randall, J. Rosenfield, and M. Rex (2002), POAM III observations of arctic ozone loss for the 1999/2000 winter, *J. Geophys. Res.*, *107*(D20), 8262, doi:10.1029/2001JD000476.

Kar, J., *et al.*, *in press*, Initial comparison of ozone and NO₂ profiles from ACE-MAESTRO with balloon and satellite data, *J. Geophys. Res.*

Livesey, N. J., W. G. Read, L. Froidevaux, J. W. Waters, M. L. Santee, H. C. Pumphrey, D. L. Wu, Z. Shippony, and R. F. Jarnot (2003), The UARS Microwave Limb Sounder version 5 data set: Theory, characterization, and validation, *J. Geophys. Res.*, *108*(D13), 4378, doi:10.1029/2002JD002273.

Lucke, R. L., *et al.* (1999), The Polar Ozone and Aerosol Measurement (POAM) III instrument and early validation results, *J. Geophys. Res.*, *104*(D15), 18,785–18,800.

Lumpe, J. D., *et al.* (1997), POAM II retrieval algorithm and error analysis, *J. Geophys. Res.*, *102*(D19), 23,593–23,614.

Lumpe, J. D., R. M. Bevilacqua, K. W. Hoppel, and C. E. Randall (2002), POAM III retrieval algorithm and error analysis, *J. Geophys. Res.*, *107*(D21), 4575, doi:10.1029/2002JD002137.

Manney, G. L., R. W. Zurek, W. A. Lahoz, R. S. Harwood, J. C. Gille, J. B. Kumer, J.L Mergenthaler, A. E. Roche, A. O'Neill, R. Swinbank, and J. W. Waters (1995a), Lagrangian transport calculations using UARS data. Part I: Passive Tracers, *J. Atmos. Sci.*, *52*, 3,049-3,068.

Manney, G. L., R. W. Zurek, L. Froidevaux, J. W. Waters, A. O'Neill, and R. Swinbank (1995b), Lagrangian transport calculations using UARS data. Part II: Ozone, *J. Atmos. Sci.*, *52*, 3069-3081.

Manney, G. L., L. Froidevaux, M. L. Santee, N. J. Livesey, J. L. Sabutis, and J. W. Waters (2003), Variability of ozone loss during Arctic winter (1991–2000) estimated from UARS Microwave Limb Sounder measurements, *J. Geophys. Res.*, *108*, 4149, doi:10.1029/2002JD002634.

Manney, G. L., K. Krüger, J. L. Sabutis, S. A. Sena, and S. Pawson (2005), The remarkable 2003–2004 winter and other recent warm winters in the Arctic stratosphere since the late 1990s, *J. Geophys. Res.*, *110*, D04107, doi:10.1029/2004JD005367.

Manney G.L., M.L. Santee, L. Froidevaux, K. Hoppel, N.J. Livesey, J.W. Waters (2006), EOS MLS observations of ozone loss in the 2004–2005 Arctic winter, *Geophys. Res. Lett.*, *33*, L04802, doi:10.1029/2005GL024494.

Massoli, P., M. Maturilli, and R. Neuber (2006), Climatology of Arctic polar stratospheric clouds as measured by lidar in Ny-A° lesund, Spitsbergen (79_N, 12_E), *J. Geophys. Res.*, *111*, D09206, doi:10.1029/2005JD005840.

Morris, G. A., J. F. Gleason, J. M. Russell III, M. R. Schoeberl, and M. P. McCormick (2002), A comparison of HALOE V19 with SAGE II V6.00 ozone observations using trajectory mapping, *J. Geophys. Res.*, *107*(D13), 4177, doi:10.1029/2001JD000847.

Müller, R., J. Grooß, D. S. McKenna, P. J. Crutzen, C. Brühl, J. M. Russell III, and A. F. Tuck (1997), HALOE observations of the vertical structure of chemical ozone depletion in the Arctic vortex during winter and early spring 1996–1997, *Geophys. Res. Lett.*, *24*, 2,717–2,720.

Müller, R., S. Tilmes, P. Konopka, J.-U. Grooß, and H.-J. Jost (2005), Impact of mixing and chemical change on ozone-tracer relations in the polar vortex, *Atmos. Chem. Phys.*, *5*, 3,139–3,151.

Nakajima, H., et al. (2002), Characteristics and performance of the Improved Limb Atmospheric Spectrometer (ILAS) in orbit, *J. Geophys. Res.*, 107, 8213, doi:10.1029/2001JD001439.

Nakajima, H., et al. (2006), Measurements of ClONO₂ by the Improved Limb Atmospheric Spectrometer (ILAS) in high-latitude stratosphere: New products using version 6.1 data processing algorithm, *J. Geophys. Res.*, 111, D11S09, doi:10.1029/2005JD006441.

Naujokat, B., K. Krüger, K. Matthes, J. Hoffmann, M. Kunze, and K. Labitzke (2002), The early major warming in December 2001 – exceptional?, *Geophys. Res. Lett.*, 29(21), 2023, doi:10.1029/2002GL015316.

Pawson, S., B. Naujokat, and K. Labitzke (1995), On the polar stratospheric cloud formation potential of the northern stratosphere, *J. Geophys. Res.*, 100(D11), 23,215–23,226.

Pawson, S., and B. Naujokat (1999), The cold winters of the middle 1990s in the northern lower stratosphere, *J. Geophys. Res.*, 104(D12), 14,209–14,222.

Plumb, R. A., D. W. Waugh, and M. P. Chipperfield (2000), The effects of mixing on tracer relationships in the polar vortices, *J. Geophys. Res.*, 105(D8), 10,047–10,062.

Randall, C. E., et al. (1995), Preliminary results from POAM II: Stratospheric ozone at high northern latitudes, *Geophys. Res. Lett.*, 22(20), 2733–2736.

Randall, C. E., et al. (2002), Reconstruction of three-dimensional ozone fields using POAM III during the SOLVE, *J. Geophys. Res.*, 107, 8299, doi:10.1029/2001JD000471.

Randall, C. E., et al. (2003), Validation of POAM III ozone: Comparisons with ozonesonde and satellite data, *J. Geophys. Res.*, 108, 4367, doi:10.1029/2002JD002944.

Reber, C. A. (1993), The upper atmosphere research satellite (UARS), *Geophys. Res. Lett.*, 20(12), 1215–1218.

Rex, M., et al., (1997), Prolonged stratospheric ozone loss in the 1995-96 Arctic winter, *Nature*, 389, 835-838.

Rex, M., R. J. Salawitch, P. von der Gathen, N. R. P. Harris, M. P. Chipperfield, and B. Naujokat (2004), Arctic ozone loss and climate change, *Geophys. Res. Lett.*, 31, L04116, doi:10.1029/2003GL018844.

Rusch, D. W., et al. (1997), Validation of POAM ozone measurements with coincident MLS, HALOE, and SAGE II observations, *J. Geophys. Res.*, 102(D19), 23,615–23,628.

Russell, J. M., III, L. L. Gordley, J. H. Park, S. R. Drayson, W. D. Hesketh, R. J. Cicerone, A. F. Tuck, J. E. Frederick, J. E. Harries, and P. J. Crutzen (1993), The Halogen Occultation Experiment, *J. Geophys. Res.*, 98(D6), 10,777–10,797.

Salawitch, R. J. et al. (2002), Chemical loss of ozone during the Arctic winter of 1999/2000: An analysis based on ballone-borne observations, *J. Geophys. Res.*, 107, 8269, doi:10.1029/2001JD000620.

Salawitch, R. J., D. K. Weisenstein, L. J. Kovalenko, C. E. Sioris, P. O. Wennberg, K. Chance, M. K. W. Ko, and C. A. McLinden (2005), Sensitivity of ozone to bromine in the lower stratosphere, *Geophys. Res. Lett.*, 32, L05811, doi:10.1029/2004GL021504.

Santee, M. L., G. L. Manney, W. G. Read, L. Froidevaux, and J. W. Waters (1996), Polar vortex conditions during the 1995–96 Arctic winter: MLS ClO and HNO₃, *Geophys. Res. Lett.*, 23(22), 3207–3210.

Sasano, Y., M. Suzuki, T. Yokota, and H. Kanzawa (1999), Improved Limb Atmospheric Spectrometer (ILAS) for stratospheric ozone layer measurements by solar occultation technique, *Geophys. Res. Lett.*, 26(2), 197–200.

Schoeberl, M. R., et al. (2006), Chemical observations of a polar vortex intrusion, *J. Geophys. Res.*, 111, D20306, doi:10.1029/2006JD007134.

Singleton, C., C. E. Randall, M. P. Chipperfield, S. Davies, W. Feng, R. M. Bevilacqua, K. W. Hoppel, M. D. Fromm, G. L. Manney, and V. L. Harvey (2005), 2002-2003 Arctic Ozone Loss Deduced from POAM III Satellite Observations and the SLIMCAT Chemical Transport Model, *Atmos. Chem. Phys.*, 5, 597-609, SRef-ID: 1680-7324/acp/2005-5-597.

Singleton, C. S., et al. (2007), Quantifying Arctic ozone loss during the 2004–2005 winter using satellite observations and a chemical transport model, *J. Geophys. Res.*, 112, D07304, doi:10.1029/2006JD007463.

Sugita, T., et al. (2005), Assessment of Improved Limb Atmospheric Spectrometer (ILAS) version 6 data quality: Measurements of stratospheric O₃, HNO₃, NO₂, N₂O, CH₄, H₂O, and aerosol extinction coefficient, *ILAS Proj. Rep. 1*, Natl. Inst. for Environ. Stud., Tsukuba, Japan. (Available at http://www-ilas.nies.go.jp/DHF/Manual/ILAS_v6_tech_report.pdf)

Thomason, L. W., and G. Taha (2003), SAGE III aerosol extinction measurements: Initial results, *Geophys. Res. Lett.*, 30, 1631, doi:10.1029/2003GL017317.

Walker, K. A., C. E. Randall, C. R. Trepte, C. D. Boone, and P. F. Bernath (2005), Initial validation comparisons for the Atmospheric Chemistry Experiment (ACE-FTS), *Geophys. Res. Lett.*, 32, L16S04, doi:10.1029/2005GL022388.

Tilmes, S., R. Müller, J.-U. Grooß, M. Höpfner, G. C. Toon, and J. M. Russell III (2003), Very early chlorine activation and ozone loss in the Arctic winter 2002–2003, *Geophys. Res. Lett.*, 30(23), 2201, doi:10.1029/2003GL018079.

Tilmes S., R. Müller, J.-U. Grooß, and J.M. Russell III (2004), Ozone loss and chlorine activation in the Arctic winters 1991-2003 derived with the tracer-tracer correlations, *Atmos. Chem. Phys.*, 4, 2181-2213.

Tilmes, S., R. Müller, A. Engel, M. Rex, and J. M. Russell III (2006), Chemical ozone loss in the Arctic and Antarctic stratosphere between 1992 and 2005, *Geophys. Res. Lett.*, 33, L20812, doi:10.1029/2006GL026925.

von Hobe, M., et al. (2006), Severe ozone depletion in the cold Arctic winter 2004–05, *Geophys. Res. Lett.*, 33, L17815, doi:10.1029/2006GL026945.

Walker, K.A., C.E. Randall, C.R. Trepte, C.D. Boone, and P.F. Bernath (2005), Initial validation comparisons for the Atmospheric Chemistry Experiment (ACE-FTS), *Geophys. Res. Lett.*, 32, L16S04, doi: 10.1029/2005GL022388.

Wang, H. J., D. M. Cunnold, L. W. Thomason, J. M. Zawodny, and G. E. Bodeker (2002), Assessment of SAGE version 6.1 ozone data quality, *J. Geophys. Res.*, 107(D23), 4691, doi:10.1029/2002JD002418.

Wang, H.-J., D. M. Cunnold, C. Trepte, L. W. Thomason, and J. M. Zawodny (2006), SAGE III solar ozone measurements: Initial results, *Geophys. Res. Lett.*, *33*, L03805, doi:10.1029/2005GL025099.

Waters, J.W., et al. (2006), The Earth Observing System Microwave Limb Sounder (EOS MLS) on the Aura satellite, *IEEE Trans. Geosci. Remote Sens.*, *44*, 1,075–1,092.

WMO (World Meteorological Organization), Scientific Assessment of Ozone Depletion: 2002, Global Ozone Research and Monitoring Project – Report No. 47, 498 pp., Geneva, 2003.

WMO (World Meteorological Organization), *Scientific Assessment of Ozone Depletion: 2006*, Global Ozone Research and Monitoring Project—Report No. 50, 572 pp., Geneva, Switzerland, 2007.

11. Figure Captions

Figure 1. The equivalent latitude of all observations made in the polar vortex during the Arctic winters of 1994-1995 through 2004-2005 on the 475 K potential temperature surface. The values of equivalent latitude are color coded by instrument.

Figure 2. Comparison of the normalization profiles used to correct each instrument. The normalization factor for each instrument at each altitude is given by the average over all

coincidences of the ratio of the instrument O_3 to the coincident SAGE II O_3 . Error bars represent 1 sigma standard deviations of the distributions.

Figure 3. Area (10^6 km^2) where Northern Hemisphere MetO temperatures fell below T_{NAT} during the winters from 1994-1995 to 2004-2005 between the 300 K and 700 K potential temperature surfaces. The black line indicates the lowest potential temperature surface (400 K) included in the O_3 loss analyses.

Figure 4. Time-altitude sections of the average wind speed at the edge of the Arctic vortex multiplied by the normalized PV gradient (see text for more details). This vortex strength diagnostic is shown for eleven winter seasons from 1994-1995 to 2004-2005 on potential temperature surfaces ranging from 400 to 700 K.

Figure 5. Ten years of inferred Arctic ozone loss (differences (ppmv) between passive O_3 calculated by the SLIMCAT CTM and the combined satellite O_3 fields). Results correspond to daily averages over the measurement locations inside the vortex during the ten Arctic winters between 400 K and 700 K. Days with missing data or on which no instruments sampled the vortex have been filled in with a linear time interpolation. The solid black line denotes the zero contour. Data have been smoothed with a 7-day running average. White spaces in the contour plots at the end of the winter (e.g. 1999-2000) indicate that vortex observations were no longer made for the remainder of the analysis period.

Figure 6. Time series of the inferred daily average O₃ loss (ppmv) inside the vortex from the combined satellite O₃ fields for the 600 K, 500 K, 475 K, and 450 K surfaces for the ten Arctic winters.

Figure 7. As in Figure 5, but for modeled daily average O₃ loss (differences (ppmv) between passive O₃ calculated by the SLIMCAT CTM and active model O₃) during the ten Arctic winters.

Figure 8. As in Figure 6, but for modeled daily average O₃ loss (ppmv) inside the vortex at the combined satellite locations during the ten Arctic winters.

Figure 9. Scatter plot of the modeled (y axis) and inferred (x axis) O₃ loss color coded by year. The solid-black line indicates the 1:1 correlation line. Dots to the left of the line indicate that the model underestimated the O₃ loss, while dots to the right of line indicate that the model overestimated the loss.

Figure 10. Maximum IL (black) and ML (red) (top panel) and their corresponding altitudes (bottom panel) for the ten Arctic winters. Only the first year of the winter is shown on the y axis (e.g. '94' represents the '94/95' winter).

Figure 11. The average O₃ loss for the last 14 days of the analysis for the observations (black) and the model (red) on the 450 K (top panel) and 600 K (bottom panel) potential

temperature surface. Only the first year of the winter is shown on the y axis (e.g. '94' represents the '94/95' winter).

Figure 12. Daily averages of observed O_3 at the combined measurement locations inside the vortex during the ten Arctic winters. Days with missing data and days where no instruments sampled the vortex have been filled in with a time interpolation. Data have been smoothed with a 7-day running average.

Figure 13. As in Figure 12, but for modeled daily average O_3 (ppmv) inside the vortex at the combined satellite locations during the ten Arctic winters.

Figure 14. Modeled minus observed daily average O_3 (ppmv) inside the vortex at the combined satellite locations during the ten Arctic winters. Shades of red (blue) indicate an overestimation (underestimation) of the modeled O_3 . The solid black line denotes the zero contour.

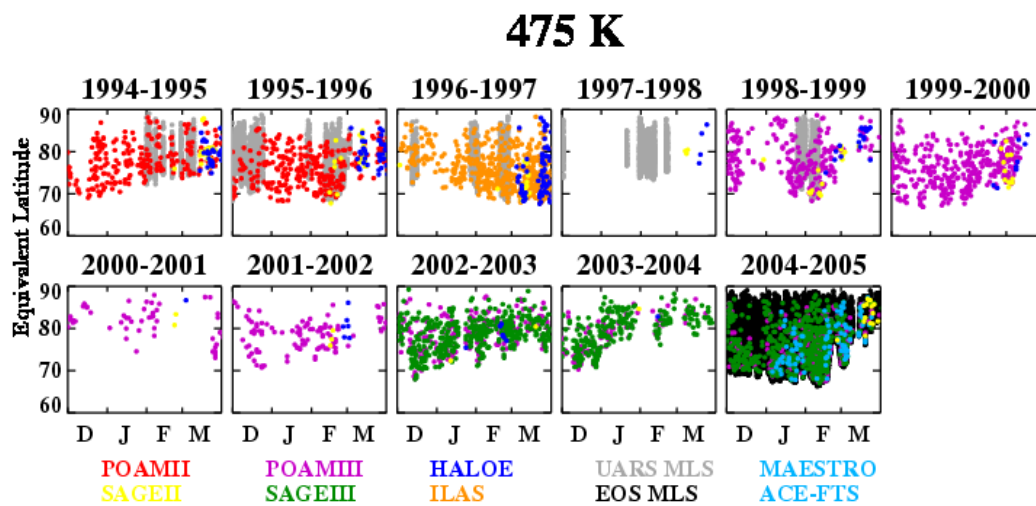


Figure 1. The equivalent latitude of all observations made in the polar vortex during the Arctic winters of 1994-1995 through 2004-2005 on the 475 K potential temperature surface. The values of equivalent latitude are color coded by instrument.

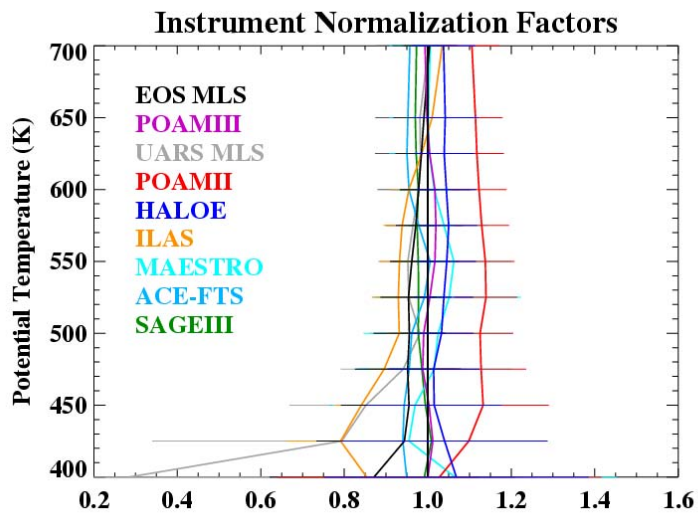


Figure 2. Comparison of the normalization profiles used to correct each instrument. The normalization factor for each instrument at each altitude is given by the average over all coincidences of the ratio of the instrument O_3 to the coincident SAGE II O_3 . Error bars represent 1 sigma standard deviations of the distributions.

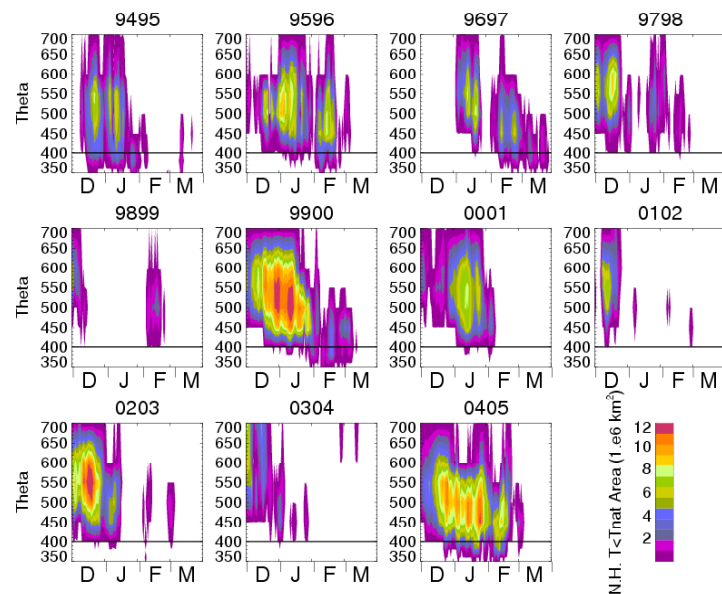


Figure 3. Area (10^6 km^2) where Northern Hemisphere MetO temperatures fell below T_{NAT} during the winters from 1994-1995 to 2004-2005 between the 300 K and 700 K potential temperature surfaces. The black line indicates the lowest potential temperature surface (400 K) included in the O_3 loss analyses.

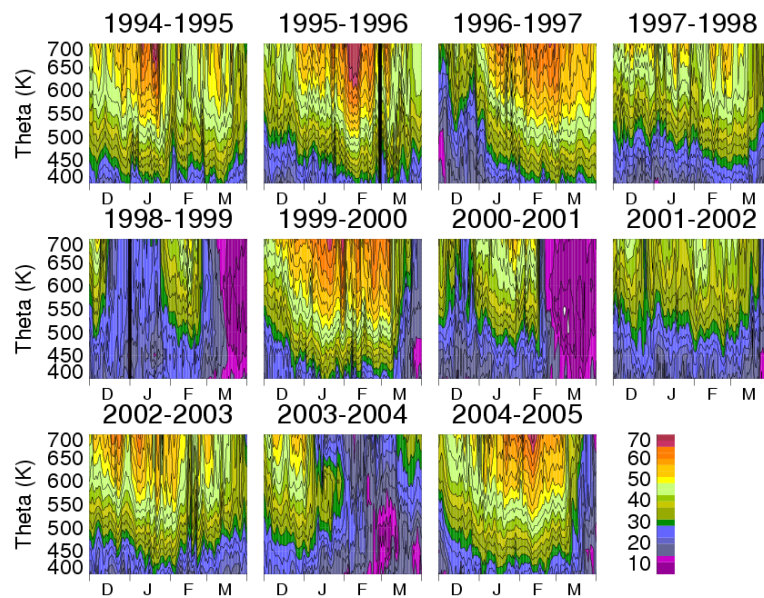


Figure 4. Time-altitude sections of the average wind speed at the edge of the Arctic vortex multiplied by the normalized PV gradient (see text for more details). This vortex strength diagnostic is shown for eleven winter seasons from 1994-1995 to 2004-2005 on potential temperature surfaces ranging from 400 to 700 K.

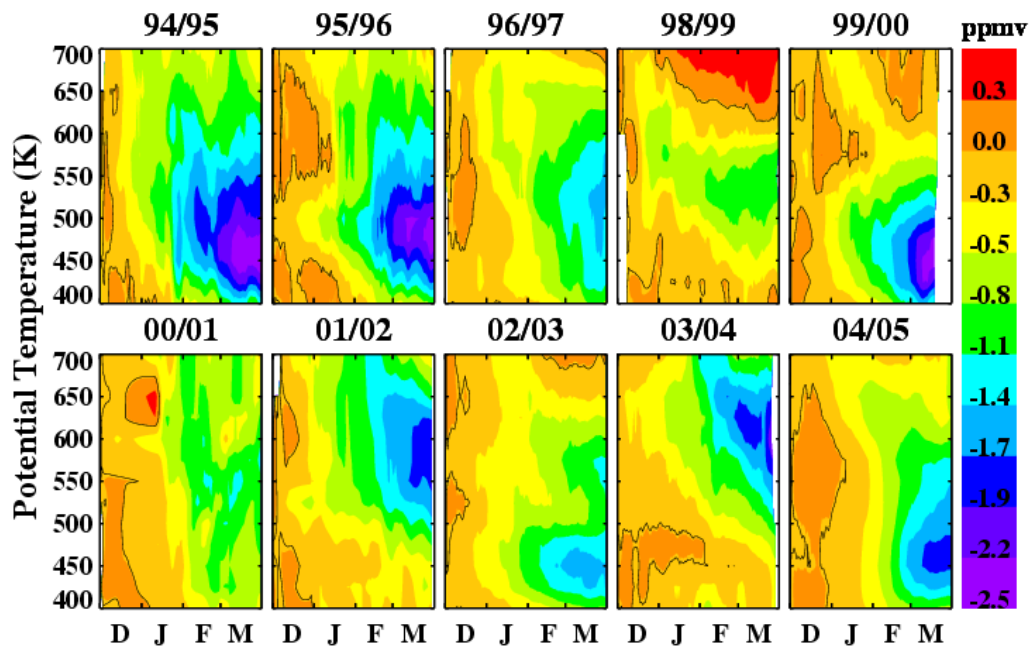


Figure 5. Ten years of inferred Arctic ozone loss (differences (ppmv) between passive O_3 calculated by the SLIMCAT CTM and the combined satellite O_3 fields). Results correspond to daily averages over the measurement locations inside the vortex during the ten Arctic winters between 400 K and 700 K. Days with missing data or on which no instruments sampled the vortex have been filled in with a linear time interpolation. The solid black line denotes the zero contour. Data have been smoothed with a 7-day running average. White spaces in the contour plots at the end of the winter (e.g. 1999-2000) indicate that vortex observations were no longer made for the remainder of the analysis period.

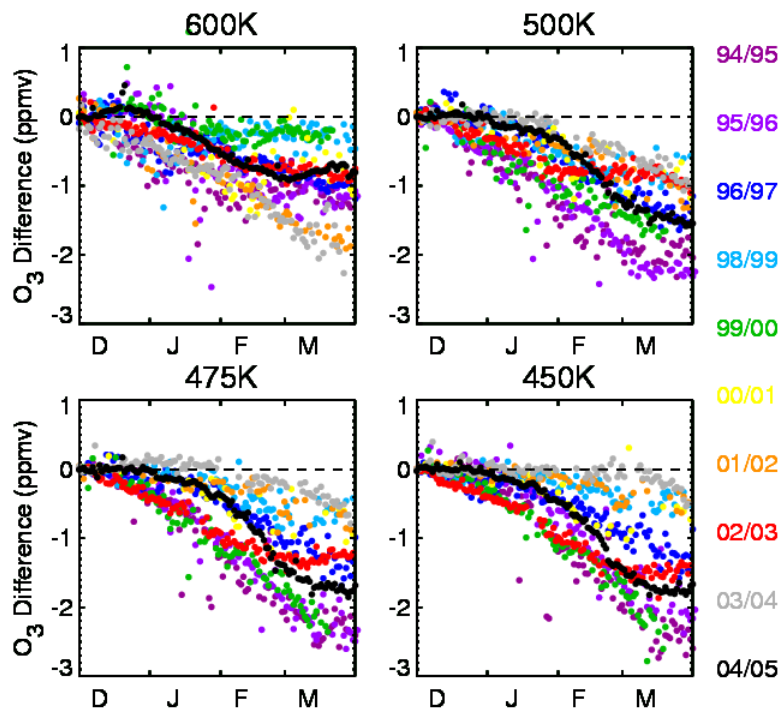


Figure 6. Time series of the inferred daily average O_3 loss (ppmv) inside the vortex from the combined satellite O_3 fields for the 600 K, 500 K, 475 K, and 450 K surfaces for the ten Arctic winters.

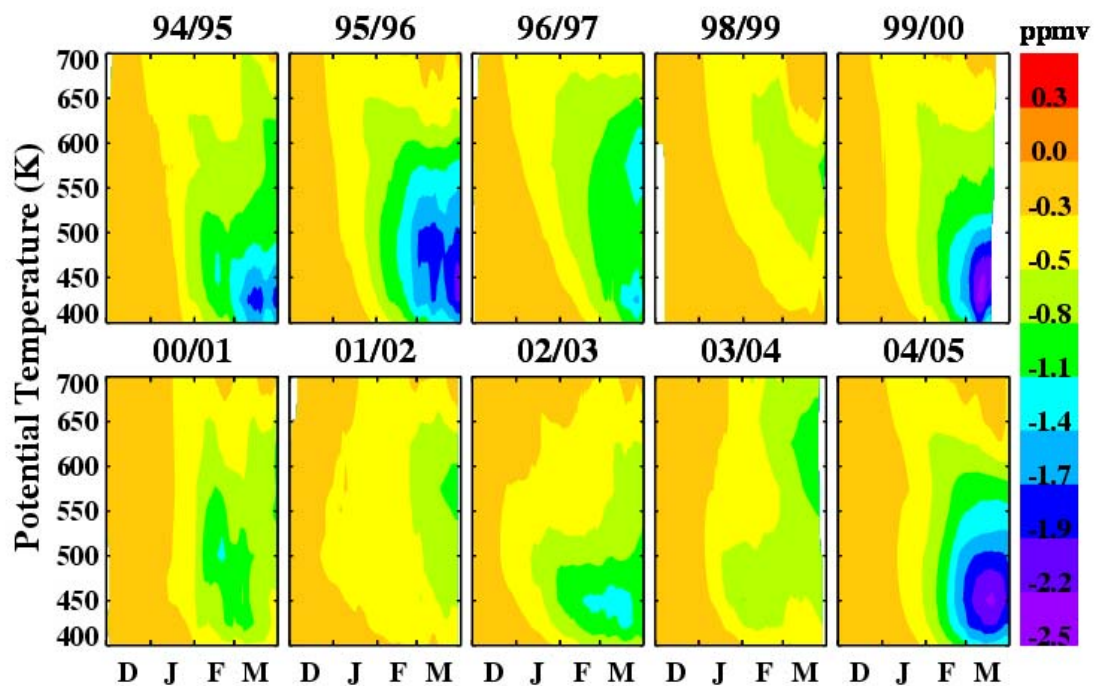


Figure 7. As in Figure 5, but for modeled daily average O₃ loss (differences (ppmv) between passive O₃ calculated by the SLIMCAT CTM and active model O₃) during the ten Arctic winters.

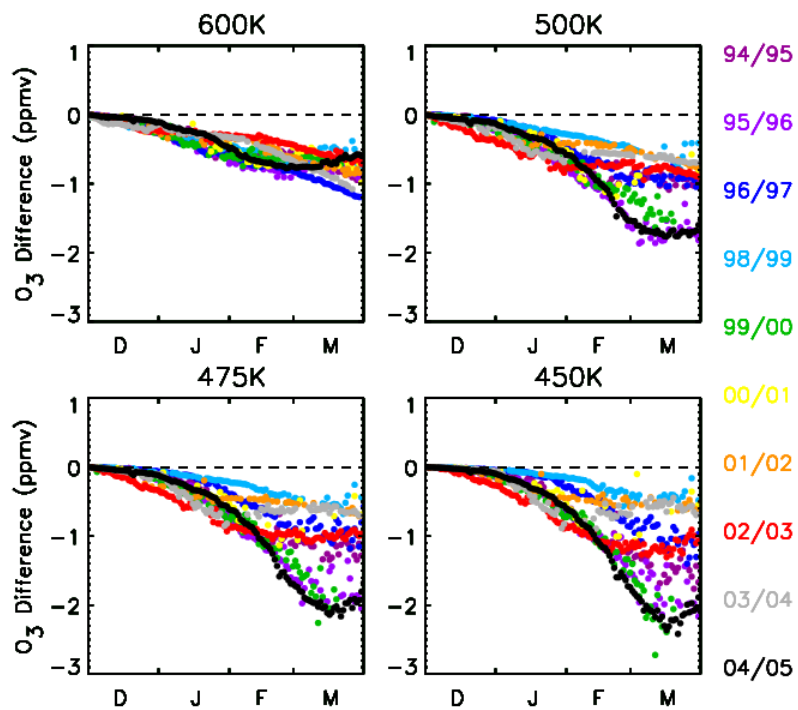


Figure 8. As in Figure 6, but for modeled daily average O₃ loss (ppmv) inside the vortex at the combined satellite locations during the ten Arctic winters.

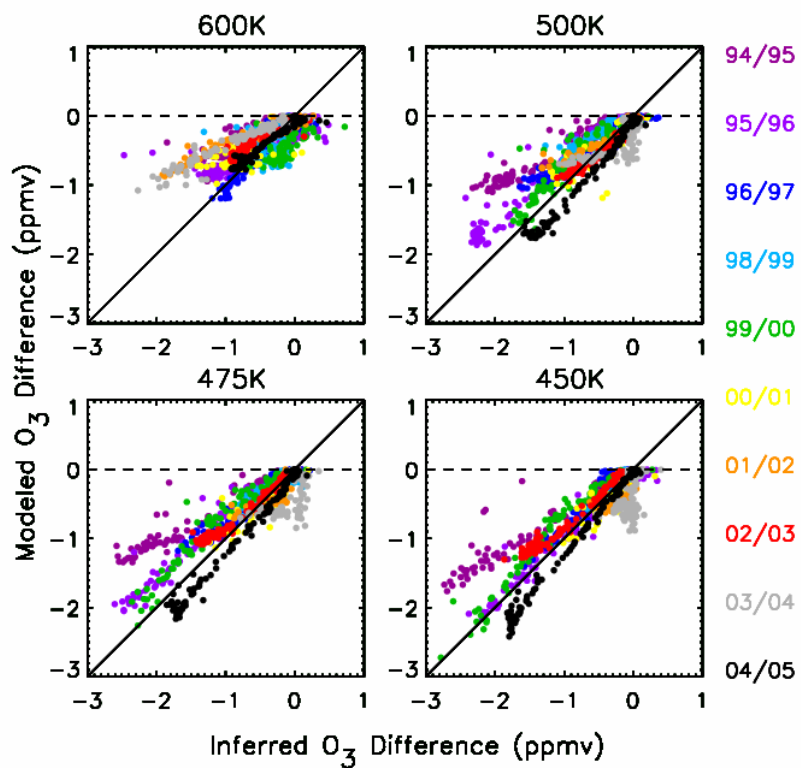


Figure 9. Scatter plot of the modeled (y axis) and inferred (x axis) O₃ loss color coded by year. The solid-black line indicates the 1:1 correlation line. Dots to the left of the line indicate that the model underestimated the O₃ loss, while dots to the right of line indicate that the model overestimated the loss.

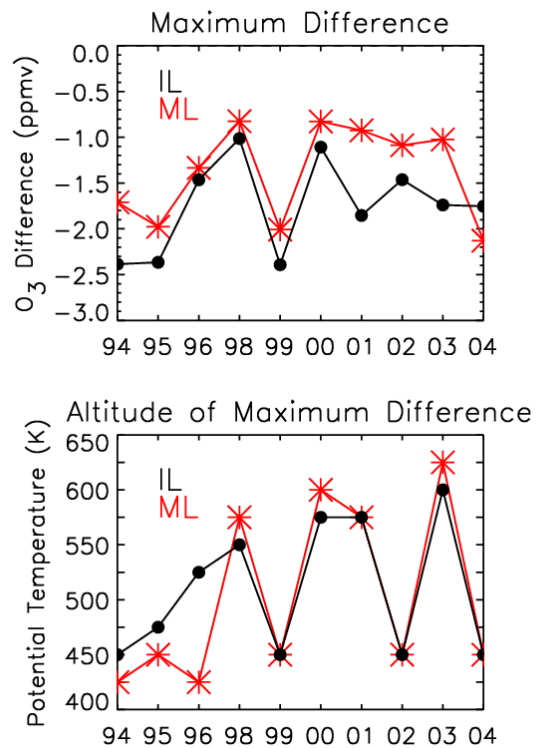


Figure 10. Maximum IL (black) and ML (red) (top panel) and their corresponding altitudes (bottom panel) for the ten Arctic winters. Only the first year of the winter is shown on the y axis (e.g. '94' represents the '94/95' winter).

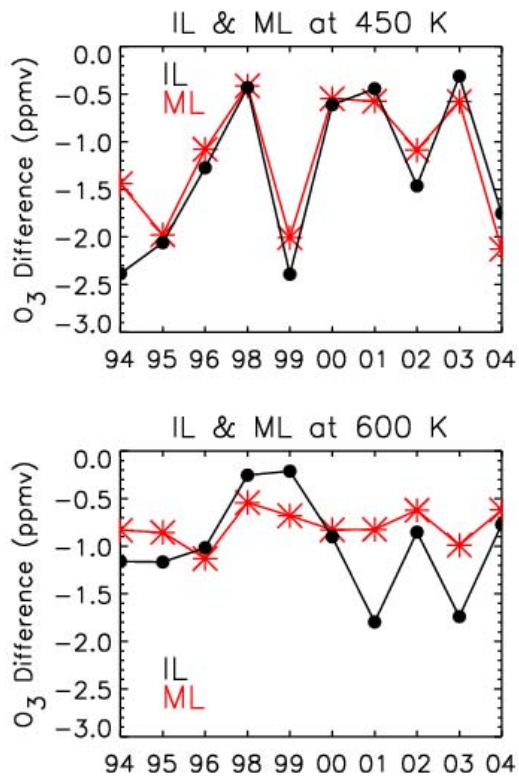


Figure 11. The average O₃ loss for the last 14 days of the analysis for the observations (black) and the model (red) on the 450 K (top panel) and 600 K (bottom panel) potential temperature surface. Only the first year of the winter is shown on the y axis (e.g. '94' represents the '94/95' winter).

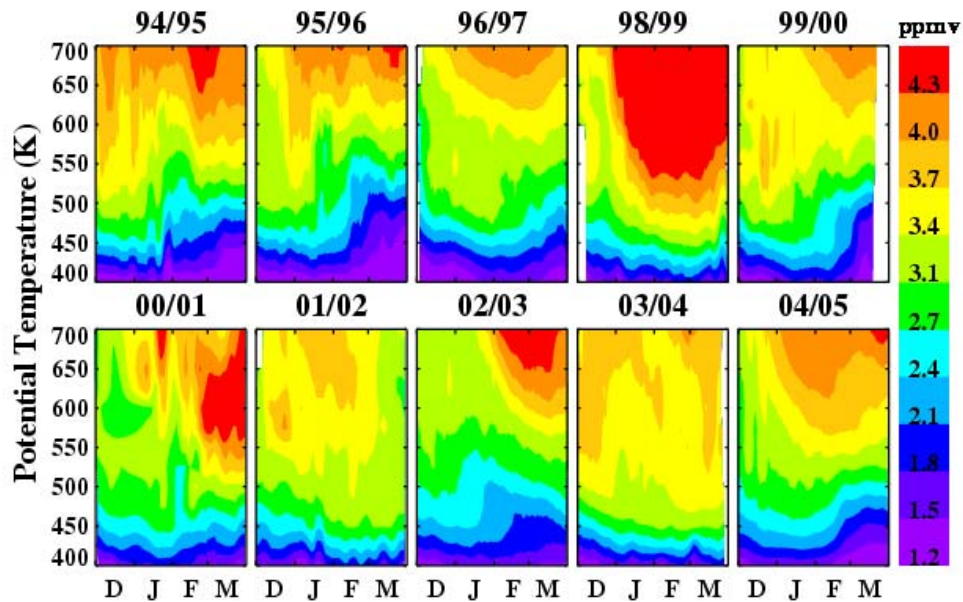


Figure 12. Daily averages of observed O_3 at the combined measurement locations inside the vortex during the ten Arctic winters. Days with missing data and days where no instruments sampled the vortex have been filled in with a time interpolation. Data have been smoothed with a 7-day running average.

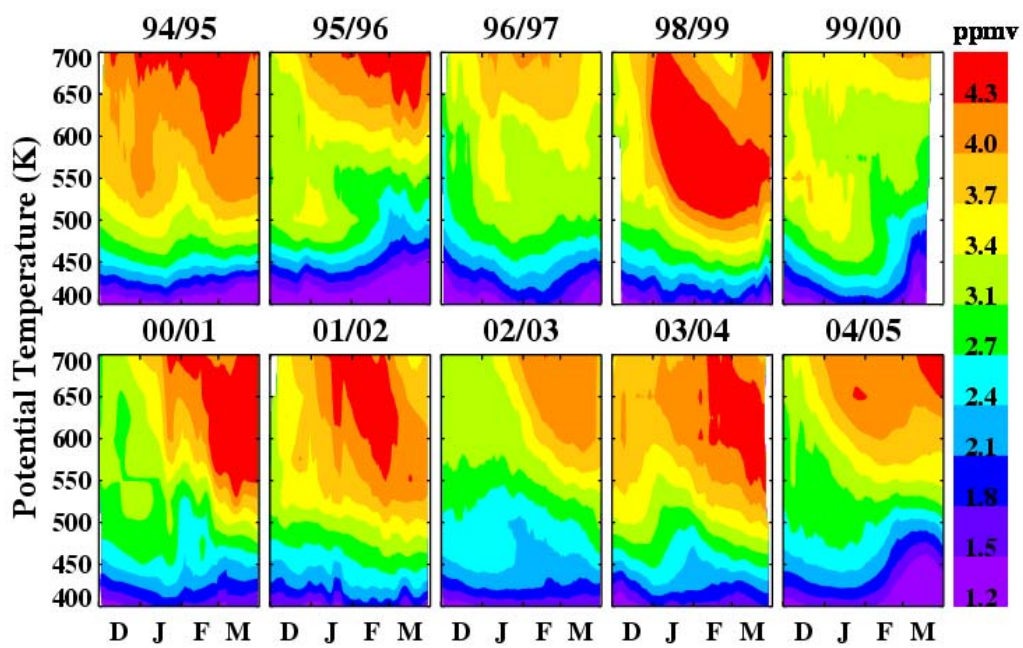
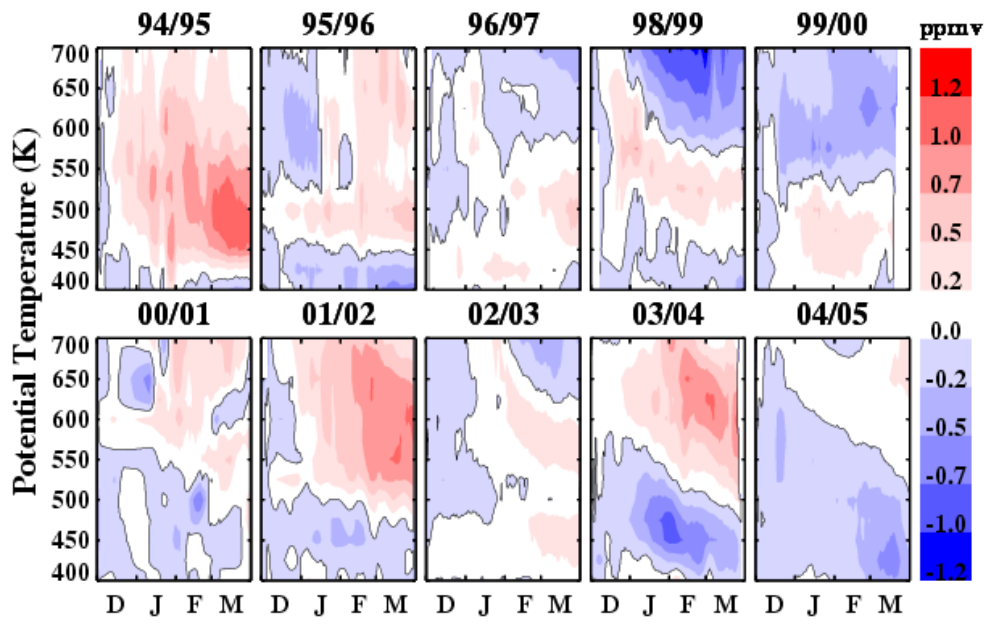


Figure 13. As in Figure 12, but for modeled daily average O_3 (ppmv) inside the vortex at the combined satellite locations during the ten Arctic winters.



1
2
3
4
5
6
7
8

Figure 14. Modeled minus observed daily average O₃ (ppmv) inside the vortex at the combined satellite locations during the ten Arctic winters. Shades of red (blue) indicate an overestimation (underestimation) of the modeled O₃. The solid black line denotes the zero contour.